Journal of Pharmaceutical Analysis 9 (2019) 40–48

Contents lists available at ScienceDirect

Journal of Pharmaceutical Analysis

journal homepage: www.elsevier.com/locate/jpa
www.sciencedirect.com

Original Article

New approaches to identification and characterization of tioconazole in raw material and in pharmaceutical dosage forms

Natalia L. Calvo [a,b,*], Vera A. Alvarez [c], María C. Lamas [a,d], Darío Leonardi [a,d,*]

[a] Instituto de Química Rosario (IQUIR, CONICET-UNR), Suipacha 531, Rosario S2002LRK, Argentina
[b] Área Análisis de Medicamentos, Facultad de Ciencias Bioquímicas y Farmacéuticas, Universidad Nacional de Rosario, Suipacha 531, Rosario S2002LRK, Argentina
[c] Grupo de Materiales Compuestos Termoplásticos (CoMP), Instituto de Investigaciones de Ciencia y Tecnología de Materiales (INTEMA, CONICET-UNMdP), Colón 10890, Mar del Plata 7600, Argentina
[d] Área Técnica Farmacéutica, Facultad de Ciencias Bioquímicas y Farmacéuticas, Universidad Nacional de Rosario, Suipacha 531, Rosario S2002LRK, Argentina

ARTICLE INFO

Article history:
Received 21 August 2018
Received in revised form
21 November 2018
Accepted 22 November 2018
Available online 23 November 2018

Keywords:
Tioconazole
Identification
Characterization
Pharmaceutical dosage forms
Spectroscopic methods

ABSTRACT

Tioconazole (TCZ), a broad-spectrum antifungal agent, has significant activity against *Candida albicans* and other *Candida* species, and therefore, it is indicated for the topical treatment of superficial mycoses. The main goal of this work is to report an exhaustive identification and characterization procedure to improve and facilitate the online quality control and continuous process monitoring of TCZ in bulk material and loaded in two different dosage forms: ovules and nail lacquer. The methodologies were based on thermal (differential scanning calorimetry (DSC), melting point, and thermogravimetry (TG)), spectroscopic (ultraviolet (UV), Raman, near infrared (NIR), infrared spectroscopy coupled to attenuated total reflectance (FTIR-ATR), and nuclear magnetic resonance (NMR)), microscopic and X-ray diffraction (XRD). The TCZ bulk powder showed a high crystallinity, as observed by XRD, with a particles size distribution (3–95 μm) resolved by microscopic measurements. TCZ melting point (82.8 °C) and a degradation peak centered at 297.8 °C were obtained by DSC and DTG, respectively. An unambiguous structure elucidation of TCZ was obtained by mono- and two- dimensional ^{1}H and ^{13}C NMR spectral data analysis. The FTIR-ATR, Raman and NIR spectra of both the raw material and the commercial products were analyzed and their characteristic bands were tabulated. The best methods for TCZ identification in ovules were DSC, TG, XRD, NIR and Raman, while NIR and FTIR-ATR were the most appropriate techniques to analyze it in the nail lacquer. DSC, TG, DRX, Raman, FTIR-ATR and NIR spectroscopy are effective techniques to be used in online process analysis, because they do not require sample preparation, and they are considerably sensitive to analyze complex samples.

1. Introduction

On line quality control and continuous process monitoring have received increasing attention, mainly to decrease production time, reduce human errors, prevent product rejections and improve efficiency. The manufacturing process frequently requires the ongoing physicochemical analysis of the product. In this regard, pharmaceutical drug characterization and identification can be performed by several analytical techniques [1–3]. Usually, the preferred approach is the use of combined techniques to achieve a better overall understanding of the properties of the active pharmaceutical ingredient (API). In the last decades, spectroscopic analyses have been employed to identify APIs even in biological materials [4] and complex matrices to rule out adulterations and fraudulent products [5]. Among spectroscopic analyses, Fourier transformed infrared spectroscopy coupled to attenuated total reflectance (FTIR-ATR) [6], near infrared (NIR) [7] and Raman [8] are the major techniques applied in green analytical chemistry. These techniques are non-destructive, allow the analysis of liquid, solid, and semi-solid samples, allow the direct measurement of untreated samples, and do not produce hazardous wastes [9]. On the other hand, nuclear magnetic resonance (NMR) spectroscopy has evolved into an irreplaceable approach for pharmaceutical quality assessment, currently playing a critical role in unequivocal

Peer review under responsibility of Xi'an Jiaotong University.
* Corresponding authors at: Instituto de Química Rosario (IQUIR, CONICET-UNR), Suipacha 531, Rosario S2002LRK, Argentina.
E-mail addresses: calvo@iquir-conicet.gov.ar (N.L. Calvo), leonardi@iquir-conicet.gov.ar (D. Leonardi).

https://doi.org/10.1016/j.jpha.2018.11.006

structure identification as well as in structural confirmation (qualitative detection), which enables the understanding of the underlying mechanisms of the formation of process and/or degradation impurities [10]. NMR can provide qualitative information, without the need for standards of the unknown compounds [11]. Thermogravimetry (TG) and differential scanning calorimetry (DSC) are useful techniques that have been successfully applied in the pharmaceutical industry to reveal important information regarding the physicochemical properties of drug and excipient molecules such as polymorphism, stability, purity, and formulation compatibility among others [12–15].

Tioconazole (TCZ), 1-[2-[(2-chloro-3-thienyl)methoxyl]-2-(2,4-dichlorophenyl)ethyl]-1H-imidazole, is a broad-spectrum antifungal agent against dermatophytes, yeasts of the genus *Candida*, as well as some *Chlamydia, Trichomonads* and some gram-positive bacteria [16].

TCZ has greater fungicidal activity than clotrimazole, econazole, ketoconazole, and miconazole against *Candida albicans* and other *Candida* species; therefore, it is used for the topical treatment of superficial mycoses, especially those resulting from fungal infections of the skin and nails [17], and for the treatment of vaginal candidiasis [18]. TCZ monograph is included in Argentinian Pharmacopoeia [19], United Stated Pharmacopoeia (USP) [20] and British Pharmacopoeia (BP) [21], where the bulk drug identification is by infrared spectroscopy (IR), thin-layer chromatography and HPLC. With the exception of IR identification tests for bulk drug, these methodologies require skilled manpower and demand the use of significant amounts of organic solvents. Besides, they are time-consuming, poorly eco-friendly, and measurements cannot be carried out online.

Therefore, this study provides a complete insight into the physicochemical identification and structural characterization of TCZ both as bulk material and in pharmaceutical dosage forms by means of different analytical techniques, some of which are eco-friendly and also could be carried out on-line.

2. Material and methods

2.1. Chemical and reagents

TCZ raw material (purity 100.74%) of pharmaceutical grade (BP 2002) was acquired in Saporiti (Buenos Aires, Argentina). During the experiments, the drug was kept in a desiccator. Double-distilled water was used for the preparation of aqueous solutions. All other chemicals were of analytical grade. Pharmaceutical dosage forms: (1) TCZ ovule (Honguil – Raymos Laboratories, Argentina) containing TCZ 14.3% (w/w) and excipients (liquid vaseline 21.4% (w/w) and solid vaseline 64.3% (w/w)), and (2) TCZ nail lacquer (Trosyd–Pfizer Laboratories Argentina), containing TCZ 28.0% (w/w) and excipients (undecylenic acid 22.0% (w/w) and ethyl acetate 50.0% (w/w)), were acquired at a local drugstore.

2.2. Methods

2.2.1. Thermal analysis

Calorimetric determinations were performed in a Linseis PT1000 differential scanning calorimeter (Linseis Inc., New Jersey, USA), operating under a constant nitrogen flow of 8 L/h.

The samples (2 mg API and 5–6 mg commercial products) were placed in closed aluminum pans perforated with a pin-hole to equilibrate pressure from potential expansion of evolved gases or residual solvents, heated at a rate of 10 °C/min between 40 and 145 °C and cooled at a rate of 5 °C/min between 145 and 55 °C. An empty pan was used as a reference.

The melting point behavior of TCZ was also examined with an Electrothermal, model 9100 digital melting point instrument (Bibby Scientific Ltd., Staffordshire, UK). The samples were heated at 10 °C/min up to 10 °C below the temperature of interest; then, the heating rate was changed to 1 °C/min.

Thermogravimetric tests were carried out with a thermal analyzer (Model TGA Q500, Hüllhorst, Germany). Samples (around 8 mg) were heated at a constant rate of 10 °C/min from room temperature up to 600 °C under a nitrogen flow of 30 mL/min in order to avoid the thermo oxidative reactions.

2.2.2. Fourier transformed infrared spectroscopy

Infrared spectra were acquired in a Shimadzu Prestige 21 spectrometer (Shimadzu Corp., Kyoto, Japan) over a wave number range of 4000–600 cm^{-1}. ATR experiments were carried out with a diamond-based ATR accessory (GladiATR, Pike Technologies, Madison, USA) fitted with a Pike temperature control unit. An average of 20 scans was used at a 4 cm^{-1} resolution between 4000 and 600 cm^{-1} in all cases. The temperature (30 °C), the amount of sample (around 20 mg) and the pressure exerted on the sample during the measurement were standardized. Each sample was scanned three times to observe good reproducibility and the scanned measurements were averaged.

2.2.3. Near infrared spectroscopy

The near infrared spectra were measured at room temperature with a spectrometer NIRS DS2500 FOSS (FOSS, Hillerod, Dinamarca). Solid sample (700 mg) was placed in a circular quartz cell for solids, while liquid and semisolid samples (1 mL) were placed in a circular quartz cell for liquids. The NIR data were an average of 7 scans in all cases, collected in the spectral range 400–2500 nm. To achieve a sufficient signal to noise ratio, all samples were measured by triplicate and averaged.

2.2.4. Raman spectroscopy

The FT-Raman experiments were performed with a hand-held AHURA TRUSCAN instrument, operated in the range 2875–230 cm^{-1}, at a nominal resolution of 7 cm^{-1}. The laser excitation wavelength was 785 nm, using 2 cm^{-1} linewidth and monochromator spectral range of 781–1014 nm. The samples (1 cm^3) were placed in closed glass vials.

2.2.5. UV-DAD spectroscopy

The spectroscopic determinations in the UV were carried out with an Agilent 8453 UV–DAD spectrophotometer (Agilent Technologies, Santa Clara, USA), controlled by the Chemstation v. B04-02 software, at a 1 nm resolution, between 190 and 1100 nm. The determinations were performed in a quartz cuvette (10 mm optical path length) against a blank of double-distilled water.

Stock standard solutions of TCZ (200 μg/mL) were prepared in 25 mL volumetric flasks, by dissolving accurately weighed amounts of the drug in acetonitrile. The working solution (9.5 μg/mL) was prepared by transferring appropriate volumes of the stock solutions to separate 50 mL volumetric flasks and diluting with water to their mark.

2.2.6. X-ray diffraction analysis (XRD)

XRD analysis was carried out with a PAN analytical X'Pert PRO diffractometer (Netherlands) equipped with a monochromatic Cu Kα radiation source (λ = 1.5406 Å) operating at a voltage of 40 kV and current of 40 mA at a scanning rate of 0.02°/s. The scanning region of the samples (solid samples: 500 mg and liquid or semisolid samples: 1 mL) was in a 2θ range between 5° and 40°.

2.2.7. Morphology analysis and size determination by scanning electron microscopy

The particle size and morphology of raw TCZ (around 10 mg) were investigated by scanning electron microscopy (SEM, AMR

1000, Leitz, Wetzlar, Germany). TCZ powder was mounted on an aluminum sample support using conductive, double-sided adhesive tape. Samples were coated with a fine gold layer for 15 min at 70–80 mTorr in order to make them conductive before obtaining the SEM micrographs. All samples were examined using an accelerating voltage of 20 kV and magnifications of 500 ×, 1000 × and 5000 ×. SEM images were analyzed using the Image-Pro Plus (IPP) software v. 6.0 to determine an indirect estimation of the particle size. The particle size was determined by an indirect estimation using the Feret's diameter which is the distance between the two furthest points of the shape measured in a given direction. About 200 particles Feret's diameters were considered in each particle size distribution calculation [22,23].

2.2.8. Nuclear magnetic resonance (NMR)

The ^{1}H and ^{13}C NMR spectra were acquired in DMSO-d_6 in a Bruker Avance spectrometer (300.13 and 75.48 MHz for ^{1}H and ^{13}C, respectively) with tetramethylsilane (TMS) as an internal standard (Bruker BioSpin GmbH, Karlsruhe, Germany). The ^{1}H and ^{13}C NMR spectra of samples (around 10 mg TCZ) were exported in txt format. NMR signals are abbreviated as follows: s = singlet; d = doublet; dd = doublet of doublets; t = triplet and m = multiplet. The chemical shifts (δ) are reported in ppm downfield from TMS; coupling constants (J). Special 1D (DEPT 135) and 2D (COSY, HMBC and HSQC) NMR experiments were also acquired, to better ascertain H–H and C–H connectivity and proximity.

3. Results and discussion

3.1. Characterization of bulk drug

3.1.1. Thermal analysis

In the DSC analysis, TCZ exhibited a single endothermic peak (Fig. 1A), without shoulders at 82.8 °C, with an onset temperature of 77.6 °C, associated with the melting process [24]. These results were in agreement with the data recorded with the melting point apparatus (80.2–81.1 °C), and also in accordance with the literature (82 °C) [25]. The calculated melting heat was 71.17 J/g. Additionally, no recrystallization peak was observed in the corresponding cooling curve.

Regarding the thermogravimetric analysis, the entire weight loss of TCZ was observed in one single stage in the temperature range of 180–307 °C. Derivative of the residual mass as a function of temperature (DTG, Fig. 1B) displayed a degradation peak centered at around 297.8 °C.

3.1.2. Spectroscopy data

The FTIR-ATR spectrum of TCZ (Fig. 2A) was in agreement with reference of the standard TCZ (KBr disks) of BP 2010 [21].

The informative spectral ranges were examined, the characteristic peaks corresponding to ν(C=N) of the imidazol group 1562.3 cm^{-1}, δ(C–H) 1464.0 cm^{-1}, ν(C=C) 1433.1 cm^{-1}, ν(C–N) 1278.8 cm^{-1}, ν(C–O–C) 1118.7 cm^{-1}, ν(C–S) 733.0 cm^{-1} and ν(C–Cl) 626.9 cm^{-1} were identified [26,27].

Fig. 2B shows the following bands at 1112, 1394.5, 1458.5, 1634, 1717.5, 1760.5, 1793.5, 1816.5, 2152.5, 2220, 2239, 2275, 2304.5, 2339.5, 2388.5, 2417.5 and 2489.5 nm in the NIR spectrum.

The absorption in the near infrared corresponds to the overtones and bands of the combination of the fundamental vibrations observed in the middle infrared. These bands are less likely than the fundamental transitions, which causes the absorption in the NIR region to be of less intensity. Organic compounds have many vibrational modes that cause the NIR spectrum to be complex and formed by broad and ill-defined bands [28]. The intensity of absorption in the NIR region depends on the anharmonicity of the bond; the more anharmonic, the greater probability for overtones and combination bands. For this reason, the bonds C–H, N–H, and O–H are very anharmonic due to the differences in the atomic weight between the two atoms, thus being very absorbent in the NIR region. The bands of groups C=O, C–C, C–F and C–Cl, in general, have lower intensity or do not appear in the NIR region [29].

The combination bands of the CH and CH_2 groups can be observed between 2200 and 2500 nm [30], while the combination bands of the NH bonds appear in the region of 2150–2200 nm [31]. The first overtone of the CH and CH_2 stretching vibrations was found in the 1700–1800 nm region [32]. The band at 1634 nm corresponds to the first overtone of the AR-CH stretching vibrations, while the bands caused by the association of the first overtone of the CH and CH_2 stretching vibrations and its combination bands can be observed at 1350–1500 nm region. Finally, the band at 1112 nm corresponds to the second overtone of the AR-CH stretching vibrations [33,34].

Fig. 2C shows the Raman spectrum with a vibrational band at 1420.9 cm^{-1} that is assigned to the imidazole ring, whereas the

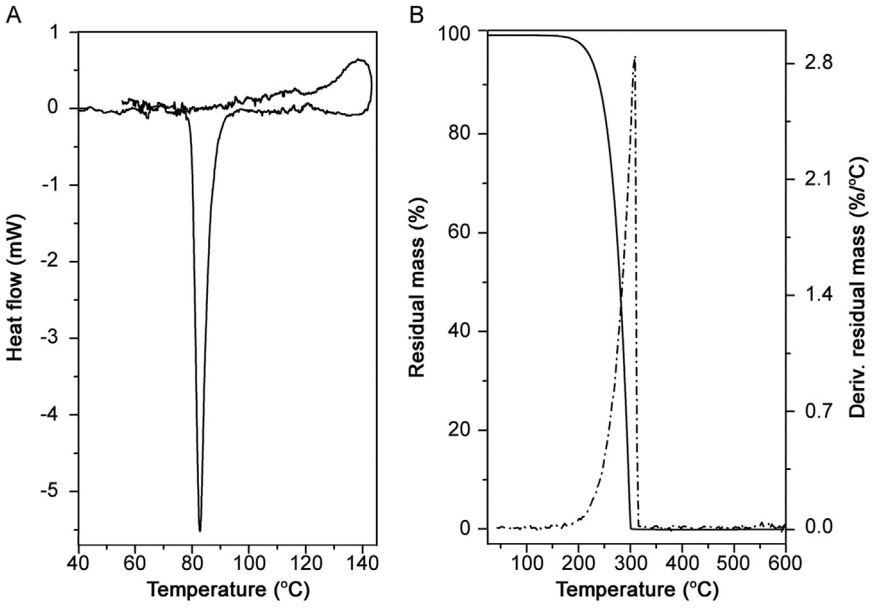

Fig. 1. Thermograms of TCZ. (A) DSC and (B) TG and DTG.

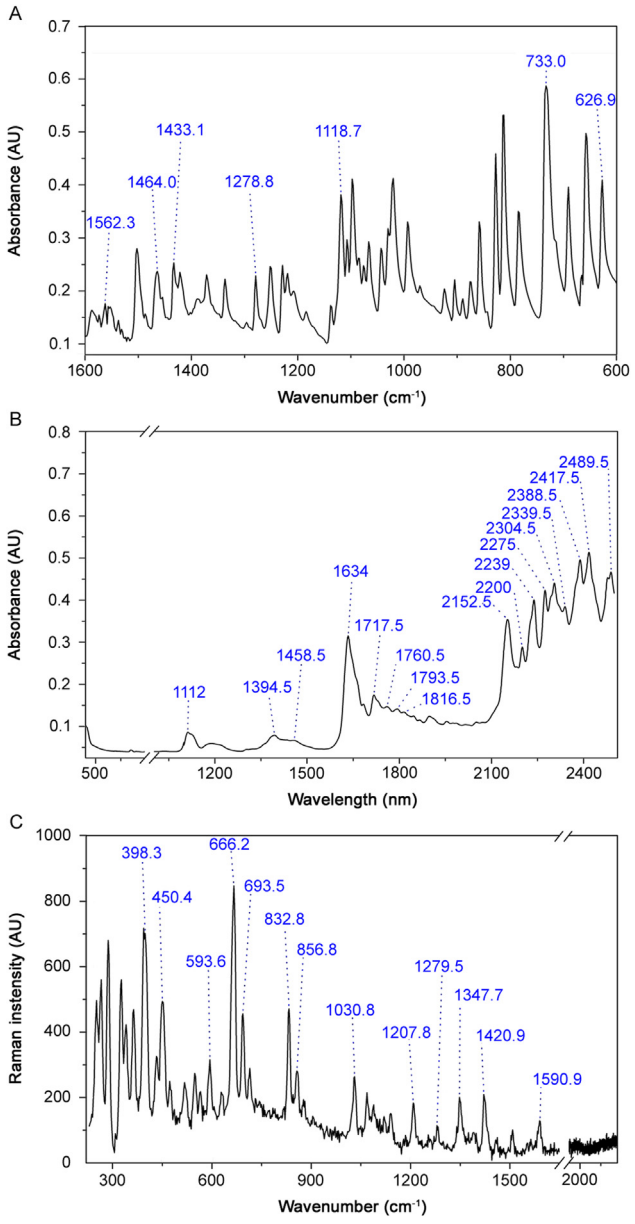

Fig. 2. (A) FTIR-ATR, (B) NIR and (C) Raman spectra of TCZ bulk drug.

bands at 593.6, 693.5, 832.8, 1030.8 and 1590.9 are ascribed to those of γ (C_4ClH_2S) chlorothiophene ring. The bands at 398.3, 450.4, 666.2, 856.8, 1207.8, 1279.5, and 1347.7 cm^{-1} refer to the δ ($C_6H_3Cl_2$) dichlorophenyl ring [35].

A stock solution of 9.5 μg/mL of TCZ was prepared in water and scanned by UV spectrophotometer to determine TCZ λmax (Fig. S1). The molecule presented two λmax, an intense band at 199 nm and a lower intensity band at 225 nm [27]. Such spectrum is similar to those observed in other imidazoles, such as sulconazole and econazole nitrate [36].

3.1.3. Crystanillity, particle size and morphology

The crystalline character of the drug was confirmed through an XRD analysis (Fig. 3). The TCZ raw material showed an intense peak at 22.33°, which is in agreement with that in a previous report [24]. In addition to the diffraction peaks indicated in Fig. 3A, peaks at 2θ around 8.71, 10.39, 13.49, 13.83, 24.61, 25.33, 26.27, 28.99, 29.39, 32.17, 32.77, and 38.59° were also observed.

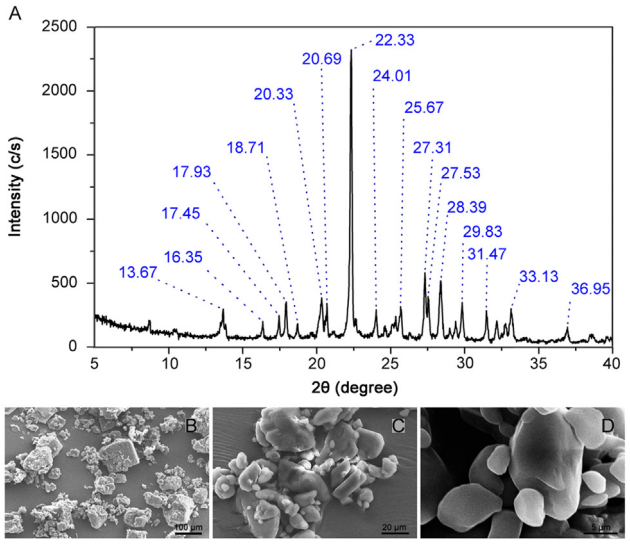

Fig. 3. Crystanillity, particle size and morphology of TCZ. (A) XRD powder pattern. SEM micrographs at (B) 200 ×, (C) 1000 ×, and (D) 5000 × magnifications.

As it can be observed in Figs. 3B-D, TCZ crystals appear as a mixture of smooth-surfaced irregular blocks of different shapes and sizes. As mentioned, particle size was determined employing the IPP software v. 6.0 which calculates the Feret's diameter from the images. Feret's diameter computed from binary images is used for estimation of length and width of dust particles [23]. The smooth surface is clearly observed when magnifications of 1000 × and 5000 × were applied. Also, a few smaller particles (3–12 μm) appearing over crystals (20–48 μm) were observed. At smaller magnification (200 ×), TCZ blocks (55–95 μm) can be distinguished.

3.1.4. NMR data analysis

Only one previous work has been carried out on the TCZ structural elucidation using NMR ^{13}C, ^{1}H, DEPT and HMBC [26]. However, some assignments require a deeper analysis, adding other NMR techniques such as HSQC and COSY, to confirm the correspondence between spectra and structure [11].

NMR ^{13}C spectrum showed 16 peaks corresponding to the 16 carbons of the molecule (Fig. 4). The DEPT 135 experiment enabled the classification of the carbon types present [37]. Eleven peaks were observed (2 with negative intensity corresponding to two carbons CH_2, and 9 with positive intensity due to CH carbons, only one of which has hybridation sp^3 at 76.39 ppm), and the

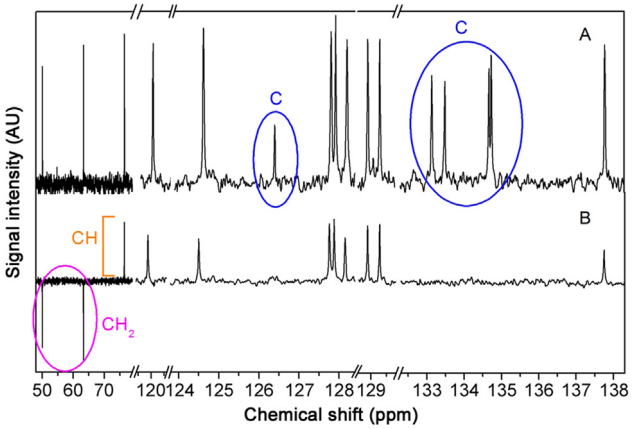

Fig. 4. NMR ^{13}C (16 peaks) and DEPT 135 spectrum (11 peaks).

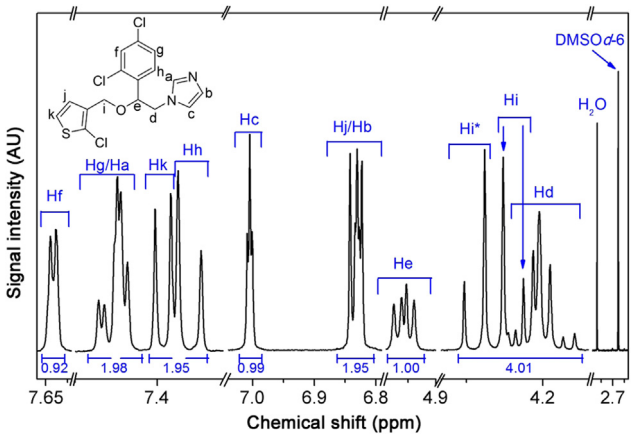

Fig. 5. ^{1}H NMR spectra of TCZ.

remaining five peaks of the ^{13}C spectrum were quaternary carbons.

The ^{1}H NMR spectra of TCZ (Fig. 5) revealed four signals of hydrogen sp^{3}, one multiplet in the region 4.24–4.19 ppm, which was assigned to Hd (2H), and two as doublets at δ 4.26 and δ 4.33 ppm (1H each). The last one, which was observed at 4.96 ppm as doublet of doublets, was assigned to He (1H, J = 4.1/ 6.7 Hz).

The signals corresponding to the imidazole group were two triplets at δ 6.83 ppm and δ 7.00 ppm (1H each, J = 1.1 Hz), which were attributed to Hb and Hc, respectively, and a signal resonating at 7.47–7.43 ppm, assigned to Ha.

Two additional doublets at δ 6.84 and δ 7.39 were attributed to Hj and Hk (1H each, J = 5.7 Hz), respectively. However, it can be observed that the Hj signal partially overlaps with Hb.

A couple of doublets at δ 7.36 (J = 8.4 Hz) and δ 7.64 (J = 2.1 Hz) were assigned to Hh and Hf, respectively. Finally, the resonances of Hg, the last signal corresponding to the dichlorephenyl group, were observed as a multiplet in the region 7.47–7.43 ppm (J = 2.2/8.1 Hz). This signal was observed to overlap with Ha.

All the C-H correlations were confirmed by 2D HSQC spectra (Fig. 6). On the other hand, long-range H-C correlations, deduced from the analysis of the HMBC spectrum, confirmed the integrity of the drug skeleton.

Table 1 displays the assignments of the ^{1}H and ^{13}C resonances of TCZ, as well as the correlations observed in the COSY (Fig. S2), HMBC (Figs. S3 and S4) and HSQC spectra (Fig. 6). Based on the analysis described above, several signals previously reported by Crisóstomo-Lucas et al. [26] were reassigned.

3.2. Identification of TCZ in pharmaceutical dosage forms

With reference to the identification of TCZ in pharmaceutical dosage forms, they were evaluated employing techniques which allow identifying TCZ in on-line quality control and continuous process.

Spectroscopic data on bulk TCZ raw material and commercial products were obtained and presented in Table 2. TCZ NIR band corresponding to 1394.5 cm^{-1} was observed at 1387.0 cm^{-1} in the

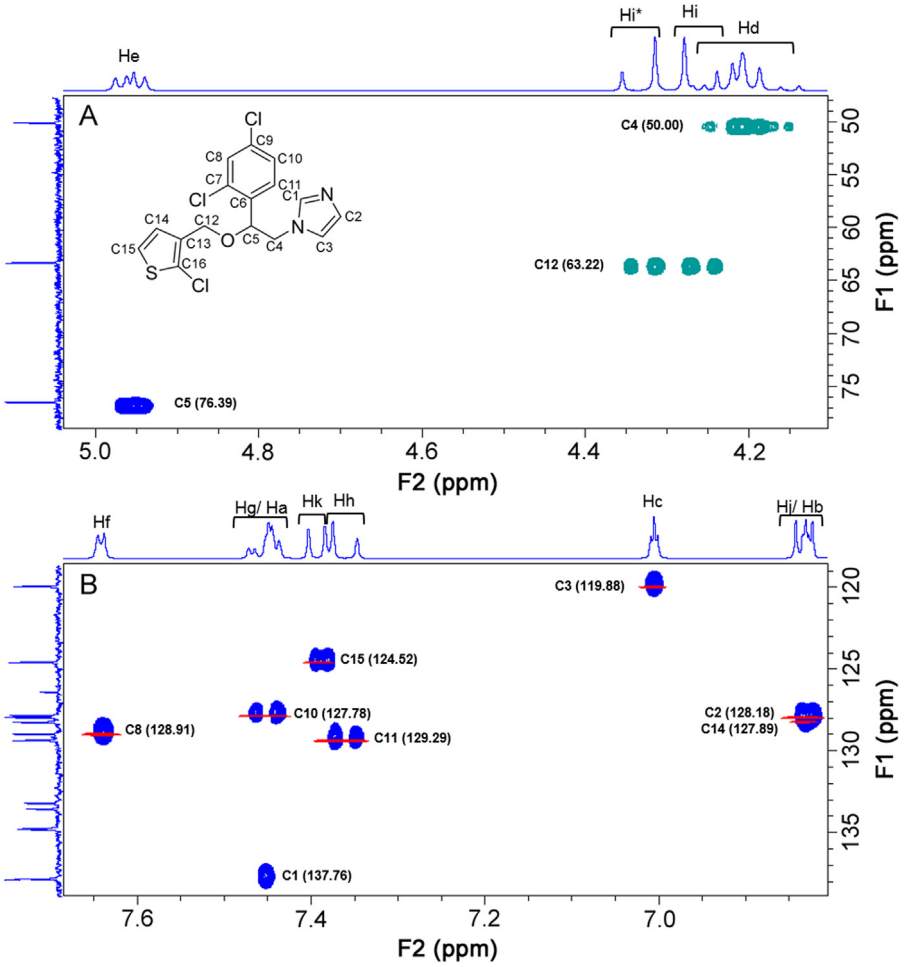

Fig. 6. 2D HSQC spectra. (A) Pure shift HSQC spectrum in the region of 48–79/5.1–4.1 ppm. (B) Pure shift HSQC (blue) and HSQC (red) in the region of 119–139/7.7–6.8 ppm.

Table 1
NMR signal assignments (H and C) of TCZ, employing 1D (^{1}H, ^{13}C and DEPT 135) and 2D (HSQC, HMBC and COSY) experiments.

H	C	^{1}H (ppm)	*J* (Hz)	^{13}C (ppm)	HSQC[a]	HMBC[b]	COSY[c]
a	1	7.47–7.43 (1H, m)		137.76 (CH, sp^2)	+	C2; C3	Hc; Hd
b	2	6.83 (1H, t)	1.1	128.18 (CH, sp^2)	+	C1; C3	Hc
c	3	7.00 (1H, t)	1.1	119.88 (CH, sp^2)	+	C1; C2; C4	Ha; Hb; Hd
d	4	4.24–4.19 (2H, m)		50.00 (CH_2, sp^3)	+	C1; C3; C5; C6	Ha; Hc; He
e	5	4.96 (1H, dd)	4.1 6.7	76.39 (CH, sp^3)	+	C4; C6; C7; C11; C12	Hd; Hh; Hi; Hi[d]
	6			134.67 (C, sp^2)			
	7			133.14 (C, sp^2)			
f	8	7.64 (1H, d)	2.1	128.91 (CH, sp^2)	+	C6; C7; C9; C10	Hg
	9			133.49 (C, sp^2)			
g	10	7.47–7.43 (1H, m)	2.2 8.1	127.78 (CH, sp^2)	+	C6; C8	Hf; Hh
h	11	7.36 (1H, d)	8.4	129.29 (CH, sp^2)	+	C5; C7; C9	Hg
i	12	4.26 (1H, d)	11.9	63.22 (CH_2, sp^3)	+	C5; C13; C14; C16	He; Hj
i[d]	12	4.33 (1H, d)	11.9	63.22 (CH_2, sp^3)	+	C5; C13; C14; C16	Hj
	13			126.34(C, sp^2)			
j	14	6.84 (1H, d)	5.7	127.89 (CH, sp^2)	+	C12; C13; C15; C16	Hi; Hk
k	15	7.39 (1H, d)	5.7	124.52 (CH, sp^2)	+	C13; C14; C16	Hj
	16			134.73(C, sp^2)			

[a] The + sign indicates that a cross-peak was observed.
[b] Carbon atoms exhibing cross-peaks with the observed H-atom.
[c] Hydrogen atoms exhibing cross-peaks with the observed H-atom.
[d] Hydrogen not equivalent.

Table 2
TCZ spectroscopic data on bulk raw material and commercial products.

Technique	TCZ	Ovule	Nail lacquer
NIR (nm)	1394.5	1392.5	1387.0
	1634.0	1634.0	1635.0
	1683.0	–	1681.5
	1717.5	1726.5	1723.0
	1760.5	1761.5	1758.0
	1816.5	1816.5	–
	2152.5	2153.0	–
	2200.0	2200.0	–
	2304.5	2311.0	2305.0
FTIR-ATR (cm^{-1})	–	721.4	–
	626.8	–	626.8
	657.7	–	657.7
	690.5	–	690.5
	733.0	733.0[a]	–
	993.3	–	993.3
	1336.7	1338.6	1336.7[a]
	1371.4	1375.3	1371.4
	1454.3[a]	1456.5	1454.3[a]
	1464.0	–	1467.8
	1562.3	–	1562.3
	1587.4	–	1589.3
	–	2848.9	2852.7
	–	2918.3	2924.1
Raman (cm^{-1})	251.6	251.6	–
	265.8	265.8	–
	287.0	287.0	–
	–	–	382.4
	450.5	450.5	–
	517.4	517.4	–
	593.7	593.7	–
	–	–	634.5
	666.3	666.3	–
	693.6	693.6	–
	833.0	831.0	–
	–	–	848.9
	1068.3	1068.3	–
	1088.7	1088.7	–

[a] Signals corresponding to a shoulder.

case of the nail lacquer and 1392.5 cm^{-1} in the ovule. In the TCZ bands at 1683.0, 1717.5, 1760.5, and 2304.5 cm^{-1}, similar slides were observed, where the values of the bands corresponding to the nail lacquer were closer to the values of TCZ powder, probably due to the greater concentration of the drug in the product. At the same time, the ovule presented the same three bands as TCZ at 1816.5, 2153.0 and 2200 cm^{-1}.

Several differences were observed when evaluating the FTIR-ATR spectra of commercial products. The nail lacquer showed a large number of bands correlated with TCZ (Table 2), whereas the ovule only presented 7 bands, only 4 of them corresponding to TCZ at 733 (present in the spectrum as a shoulder), 1338.6, 1375.3 and 1456.5 cm^{-1}. Both products showed two bands comprised between 2840 and 2950 cm^{-1} corresponding to C–H stretches of alkanes due to excipients of the formulas [38].

Raman spectroscopy could not show TCZ in the nail lacquer,

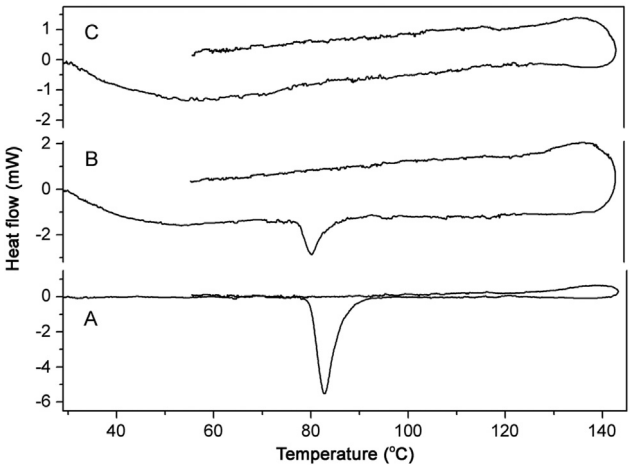

Fig. 7. DSC thermograms of (A) TCZ, and pharmaceutical dosage forms: (B) ovule and (C) nail lacquer.

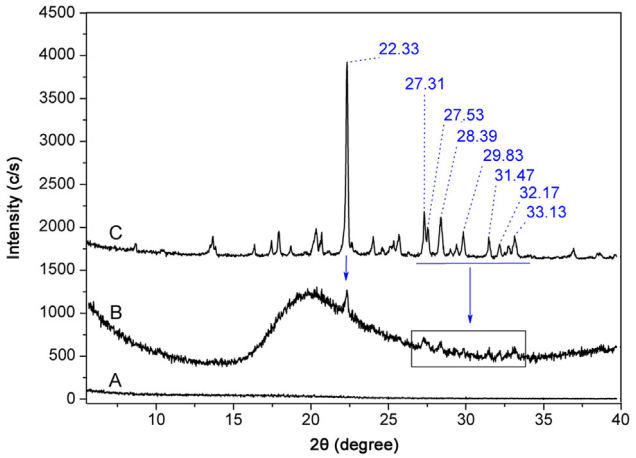

Fig. 8. XRD pattern of (A) nail lacquer, (B) ovule, and (C) TCZ.

revealing only 3 bands not related to the API, while the ovule showed 11 bands related to the TCZ with no visible shifts.

When a pharmaceutical formulation is prepared, DSC curves show changes in the fusion range, area or shape of the peaks, and disappearance or appearance of thermal events after mixing components. The obtained curves may indicate interactions or chemical reactions that must be confirmed by other analytical techniques [13].

As it is shown in Fig. 7, the DSC thermograms of the different commercially available formulations were compared with that generated by TCZ bulk powder. The thermogram of the ovule formulation presents an endothermic peak centered at 80.4 °C (enthalpy 7.29 J/g), corresponding to the melting point of TCZ, which is slightly shifted to the right, maybe due to some interactions with the excipients [13].

It could be estimated that TCZ was partially dissolved in the mixture of excipients or had an increase in the amorphization of the drug in the ovule because the heat of transition expected for TCZ in DSC curves [12,13] was reduced compared to the expected theoretical value (10.17 J/g). Nevertheless, the peak was still distinguishable from the baseline and displaced to lower temperatures, which in turn indicates that the drug (or at least part of it) is in the crystalline form [12,13].

The thermal interactions identified by DSC may be related to chemical interactions between the components of the mixtures or to innocuous physical interactions [39]. Similar shifting was observed by Verma et al. [40] when they studied glipizide–excipient compatibility. They have reported that these minor changes in the melting endotherm of drug could be due to the mixing of drug and excipient, which lowers the purity of each component in the mixture and may not necessarily indicate potential incompatibility. Moreover, Talvani et al. [41] have developed different carvedilol formulations which showed a decrease of approximately 10 °C in the drug melting peak evidencing thermal interactions between the drug and excipient. However, they have also demonstrated that the observed thermal interactions did not promote physical or chemical modifications in the drug, verifying the compatibility of carvedilol with the used pharmaceutical excipients.

Although the formulation of the nail lacquer has a high ratio of TCZ (28% (w/v)), the excipients (undecylenic acid and ethyl acetate) allowed a complete dissolution of the drug; therefore, the melting temperature near 82 °C was not observed on DSC curve. In order to evaluate the crystalline state of the drug in the pharmaceutical formulations, XRD patterns were obtained and analyzed.

The diffraction patterns of the pharmaceutical products are presented (Fig. 8) and compared with the API. The ovule showed 8 peaks corresponding to the TCZ at 22.33, 27.31, 27.53, 28.39, 29.83, 31.47, 32.17 and 33.13°, confirming that TCZ partially preserves its crystalline structure. Although this sample presents some degree of drug amorphization, it is clear that a significant fraction of crystalline drug remains in the ovule, since the main peaks of original drug crystalline phase can still be observed in the XRD spectrum [42]. On the other hand, in the diffraction pattern of the nail lacquer neither peak nor amorphous halo was observed, in agreement with the results obtained by DSC, confirming that the API is neither in a crystalline state nor in an amorphous phase. This could suggest that the drug is dissolved in the formulation.

The commercial products exhibited total mass loss in two stages (Fig. 9), unlike the TCZ that occurred in only one stage (Fig. 1B). The greatest loss of mass (92.24%) in the decomposition of ovule took place between 30 and 360 °C, with two maximum peaks of decomposition at 304.8 °C related to TCZ in accordance with the obtained results of TCZ (Fig. 1B) and 321.3 °C. Another area of mass loss (7.76%) was observed between 360 and 550 °C, which was attributed to the excipients of the commercial ovule,

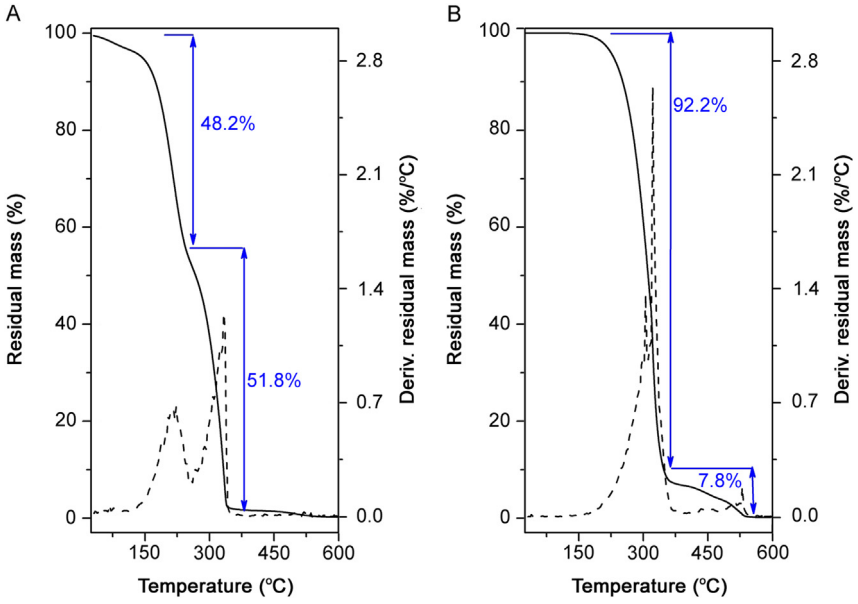

Fig. 9. TG and DTG curves of (A) nail lacquer and (B) ovule.

while in the nail lacquer (Fig. 9A), the decomposition of 48.2% occurred between 25 and 260 °C with a maximum decomposition peak at 222.4 °C. Finally, the decomposition of 51.8% of the mass occurred between 260 and 345 °C, with a maximum registered at 333.1 °C, associated to TCZ, also in accordance with the obtained results of TCZ (Fig. 1B).

4. Conclusions

A complete identification and characterization of TCZ was carried out by using several techniques, presenting NIR, DTG and SEM images of TCZ for the first time. Additionally, a TCZ structural elucidation was performed by applying different NMR techniques.

TCZ bulk powder showed a high crystallinity, as observed by XRD, with a particles size distribution resolved by SEM measurements. TCZ melting point (82.8 °C) and degradation temperature (297.8 °C) were obtained by DSC and DTG, respectively. An unambiguous elucidation structure of TCZ was obtained by mono- and two- dimensional ^{1}H and ^{13}C NMR spectral data analysis.

FTIR-ATR, Raman and NIR spectra for the raw material and the commercial products (ovule and nail lacquer) were obtained and analyzed tabulating their characteristic bands. It was found that the best methods for the identification of TCZ in the ovule were thermal ones (DSC and TG), XRD, NIR and Raman, while NIR and FTIR-ATR were the most appropriate techniques in the case of the nail lacquer. Although NMR spectroscopy is a determinant technique to elucidate the structure, DSC, TG, XRD, FTIR-ATR, NIR and Raman showed to be effective techniques to be used in online process analysis, as they require no sample preparation and have been proved to be highly sensitive to TCZ, even in complex samples.

Conflicts of interest

The authors declare that there are no conflicts of interest.

Acknowledgments

The authors gratefully acknowledge Consejo Nacional de Investigaciones Científicas y Técnicas (CONICET), Agencia Nacional de Promoción de Ciencia y Tecnología (ANPCyT), and Universidad Nacional de Rosario (UNR) for financial support. NLC is also thankful to CONICET for her fellowship. In addition, we would like to thank the staff from the English Department (Faculty of Biochemical and Pharmaceutical Science, UNR) for the language correction of the manuscript and Pilot Drug Plant by Raman spectroscopy determinations.

Appendix A. Supplementary material

Supplementary data associated with this article can be found in the online version at https://doi.org/10.1016/j.jpha.2018.11.006.

References

[1] H.G. Brittain, Physical Characterization of Pharmaceutical Solids, Marcel Dekker, New York, 1995.
[2] R. Hilfiker, Polymorphism: In the Pharmaceutical Industry, John Wiley & Sons, New Jersey, 2006.
[3] N. Satheeshkumar, S. Shantikumar, R. Srinivas, Pioglitazone: a review of analytical methods, J. Pharm. Anal. 4 (2014) 295–302.
[4] B. Kanakapura, V.K. Penmatsa, Analytical methods for determination of terbinafine hydrochloride in pharmaceuticals and biological materials, J. Pharm. Anal. 6 (2016) 137–149.
[5] A.K. Deisingh, Pharmaceutical counterfeiting, Analyst 130 (2005) 271–279.
[6] S. Filali, C. Bergamelli, M. Lamine Tall, et al., Formulation, stability testing, and analytical characterization of melatonin-based preparation for clinical trial, J. Pharm. Anal. 7 (2017) 237–243.
[7] G. Ding, Y. Hou, J. Peng, et al., On-line near-infrared spectroscopy optimizing and monitoring biotransformation process of γ-aminobutyric acid, J. Pharm. Anal. 6 (2016) 171–178.
[8] K. Gambhir, P. Singh, D.K. Jangir, et al., Thermal stability and hydration behavior of ritonavir sulfate: a vibrational spectroscopic approach, J. Pharm. Anal. 5 (2015) 348–355.
[9] S. Mukherjee, A. Gowen, A review of recent trends in polymer characterization using non-destructive vibrational spectroscopic modalities and chemical imaging, Anal. Chim. Acta 895 (2015) 12–34.
[10] V. Guvvala, V. Chidambaram Subramanian, J.S. Anireddy, et al., Novel degradation products of argatroban: isolation, synthesis and extensive characterization using NMR and LC-PDA-MS/Q-TOF, J. Pharm. Anal. 8 (2018) 86–95.
[11] R.M. Maggio, N.L. Calvo, S.E. Vignaduzzo, et al., Pharmaceutical impurities and degradation products: uses and applications of NMR techniques, J. Pharm. Biomed. Anal. 101 (2014) 102–122.
[12] M.I. Yoshida, E.C.L. Gomes, C.D.V. Soares, et al., Thermal analysis applied to verapamil hydrochloride characterization in pharmaceutical formulations, Molecules 15 (2010) 2439–2452.
[13] M. Yoshida, M. Oliveira, E. Gomes, et al., Thermal characterization of lovastatin in pharmaceutical formulations, J. Therm. Anal. Calorim. 106 (2011) 657–664.
[14] D.Q.M. Craig, M. Reading, Thermal Analysis of Pharmaceuticals, CRC press, Boca Ratón, 2006.
[15] M. Kumar, R. Bhatia, R.K. Rawal, Applications of various analytical techniques in quality control of pharmaceutical excipients, J. Pharm. Biomed. Anal. 157 (2018) 122–136.
[16] S.C. Sweetman, Martindale/Guía completa de consulta farmacoterapéutica. 2da, Edición Pharma Editores, 2006.
[17] O. Welsh, L. Vera-Cabrera, E. Welsh, Onychomycosis, Clin. Dermatol. 28 (2010) 151–159.
[18] R.N. Jones, M.J. Bale, D. Hoban, et al., In vitro antimicrobial activity of tioconazole and its concentrations in vaginal fluids following topical (vagistat-1 16.5%) application, Diagn. Microbiol. Infect. Dis. 17 (1993) 45–51.
[19] Argentinian Pharmacopoeia Commission, Argentinian Pharmacopoeia. VII Ed, Buenos Aires, 2003.
[20] US Pharmacopeial Convention, USP 36/NF 31, Rockville, 2013.
[21] British Pharmacopeia Comission, British Pharmacopeia, Londres, 2010.
[22] J. Priotti, A.V. Codina, D. Leonardi, et al., Albendazole microcrystal formulations based on chitosan and cellulose derivatives: physicochemical characterization and in vitro parasiticidal activity in Trichinella spiralis adult worms, AAPS PharmSciTech 18 (2017) 947–956.
[23] S. Dražić, N. Sladoje, J. Lindblad, Estimation of Feret's diameter from pixel coverage representation of a shape, Pattern Recognit. Lett. 80 (2016) 37–45.
[24] R.F. Ribeiro, M.H. Motta, A.P.G. Härter, et al., Spray-dried powders improve the controlled release of antifungal tioconazole-loaded polymeric nanocapsules compared to with lyophilized products, Mater. Sci. Eng. C. 59 (2016) 875–884.
[25] British Pharmacopeia Comission, Tioconazole impurity standard, 15 December 2017, ⟨https://www.pharmacopoeia.com/Catalogue/Preview?Uri=%2Fcontent%2Ffile%2Fproducts%2Fhealthandsafety%2FCat_687_GB.pdf⟩.
[26] C. Crisóstomo-Lucas, P. García-Holley, S. Hernández-Ortega, et al., Structural characterization and cytotoxic activity of tioconazole coordination compounds with cobalt(II), copper(II), zinc(II) and cadmium(II), Inorg. Chim. Acta 438 (2015) 245–254.
[27] D.S. Bisht, G.K. Bhatt, P. Kothiyal, Formulation and evaluation of nail lacquer containing tioconazole for transungual drug delivery system, Indo Am. J. Pharm. Sci. 2 (2015) 1474–1485.
[28] M. Jamrógiewicz, Application of the near-infrared spectroscopy in the pharmaceutical technology, J. Pharm. Biomed. Anal. 66 (2012) 1–10.
[29] M.B. Simpson, Near infrared spectroscopy for process analytical technology: theory, technology and implementation, Process Analytical Technology: Spectroscopic Tools and Implementation Strategies for the Chemical and Pharmaceutical Industries, John Wiley & Sons, Chichester, UK 2010, pp. 107–153.
[30] C.E. Miller, Chemical principles of near-infrared technology, Near-infrared technology in the agricultural and food industries, Phil Williams, Karl Norris, St Paul, 2001.
[31] D.-W. Sun, Infrared Spectroscopy for Food Quality Analysis and Control, Academic Press, Dublin, 2009.
[32] J.S. Shenk, J.J. Workman, M.O. Westerhaus, Application of NIR spectroscopy to agricultural products, Pract. Spectrosc. Ser. (2001) 419–474.
[33] J. Drennen, R. Lodder, Advances in Near-Infrared Measurements, JAI Press Inc., Greenwich, 1993.
[34] H.W. Siesler, Basic principles of near-infrared spectroscopy, D.A. Burns, E.W. Ciurczak, Handbook of Near-Infrared Analysis, Third ed. CRC press, Boca Ratón 2007, pp. 25–38.
[35] E.-M. Cho, E.-O. Ganbold, A.T.N. Lam, et al., Physicochemical characterization of the structure and desorption relationship of tioconazole-assembled gold nanoparticles investigated by density functional theory and Raman spectroscopy, Colloids Surf. A Physicochem. Eng. Asp. 486 (2015) 45–52.
[36] J. Kujawski, K. Czaja, E. Jodłowska, et al., Structural and spectroscopic properties of econazole and sulconazole–experimental and theoretical studies, J. Mol. Struct. 1119 (2016) 250–258.
[37] N. Kumar, S.R. Devineni, P.R. Gajjala, et al., Synthesis, isolation, identification and characterization of new process-related impurity in isoproterenol hydrochloride by HPLC, LC/ESI-MS and NMR, J. Pharm. Anal. 7 (2017) 394–400.
[38] Y. Lee, E.-A. You, Y.-G. Ha, Facile one-step construction of covalently networked, self-healable, and transparent superhydrophobic composite films, Appl. Surf. Sci. 445 (2018) 368–375.

[39] R. Ferreira-Nunes, T. Gratieri, G.M. Gelfuso, et al., Mixture design applied in compatibility studies of catechin and lipid compounds, J. Pharm. Biomed. Anal. 149 (2018) 612–617.
[40] R.K. Verma, S. Garg, Selection of excipients for extended release formulations of glipizide through drug-excipient compatibility testing, J. Pharm. Biomed. Anal. 38 (2005) 633–644.
[41] A. Talvani, M.T. Bahia, L.C.L. de Sá-Barreto, et al., Carvedilol: decomposition kinetics and compatibility with pharmaceutical excipients, J. Therm. Anal. Calorim. 115 (2014) 2501–2506.
[42] L.A. Pinho, S.G. Lima, L.F. Malaquias, et al., Improvements of theobromine pharmaceutical properties using solid dispersions prepared with newfound technologies, Chem. Eng. Res. Des. 132 (2018) 1193–1201.